Western Michigan University

The Hilltop Review

Volume 7
Issue 1 *Winter 2014*

Article 10

December 2014

Advantages of a Finite Extensible Nonlinear Elastic Potential in Lattice Boltzmann Simulations

Tai-Hsien Wu
Western Michigan University

Dewei Qi
Western Michigan University

Advantages of a Finite Extensible Nonlinear Elastic Potential in Lattice Boltzmann Simulations

Cover Page Footnote
Tai-Hsien Wu acknowledges the scholarship from the Graduate College at Western Michigan University and the nomination from the Chemical and Paper Engineering Department at Western Michigan University.

Advantages of a Finite Extensible Nonlinear Elastic Potential in Lattice Boltzmann Simulations

By Tai-Hsien Wu and Dr. Dewei Qi
Department of Chemical Engineering
tai-hsien.wu@wmich.edu

1. Introduction

There are a great number of fluid-solid interaction problems in the real world such as locomotion of flagellum in the field of biology and fiber flocculation and dispersion in various industries.

Lattice Boltzmann simulation, an effective fluid simulation method, with a lattice spring model, a method to simulate solid deformation, is a powerful tool to deal with complex interactions between flexible solid structures and fluid flows. The lattice Boltzmann method has been extensively used to simulate dynamic motion of solid particles suspended in either laminar or turbulent flows. For solid domains, a coarse-grained model such as the lattice spring model (LSM) (Buxton, Verberg, Jasnow, & Balazs, 2005) has been employed to model the deformation and motion of flexible bodies in fluid flows. Recently, a generalized lattice spring model (GLSM) has been presented by considering three-body forces or angular bonds in addition to the two-body spring bonds (Wu, Guo, He, Liu, & Qi, 2014) so that the generalized lattice spring model can effectively handle bending deformation.

Both of the LSM and the GLSM only use the simplest potential, harmonic potential, to represent the bonds between adjacent particles. One of the defects of a harmonic spring is that the distance between two bonded particles can be extended infinitely if the spring force is large enough. The consequence of the defect is that the simulation may be diverged because two particles are excessively extended and overlapped when a large spring force is used for a relatively stiff solid body. To overcome the defect, a non-linear potential which is named finitely extensible nonlinear elastic (FENE) potential with Lennard-Jones potential (FENE-LJ potential), was proposed and used frequently in molecular dynamic simulations (Kremer & Grest, 1990) (Tirion, 1996). The advantage of the FENE-LJ potential is that two bonded solid particles cannot be extended too far due to an infinitely large potential well, which traps the particles. Therefore, we will borrow FENE-LJ potential to simulate dynamic behavior of flexible bodies in fluid flows within the frame of lattice Boltzmann simulation. The new solid structure model is named the generalized lattice nonlinear spring model (GLNSM). The important critical step is to identify a relationship between Young's modulus, an important property of matters to describe extension, and the GLNSM (FENE-LJ potential) since deformation and motion of a flexible body is macroscopically determined by Young's modulus. Unfortunately, to our best knowledge, how the macroscopic parameter, Young's modulus, relates to the GLNSM (FENE-LJ potential) is not revealed so far.

The main contribution of the present work is that a detailed derivation of Young's modulus from the GLNSM (FENE-LJ potential) is presented and we point out that a coefficient K in the FENE-LJ model is not directly equal to a spring constant used in the literature (Urgessa, 2007). The GLNSM (FENE-LJ potential) is used in lattice Boltzmann simulation for the first time. It is expected that the GLNSM can simulate more stiff structures in comparison to a linear harmonic spring.

In this article, Section 2 describes the GLNSM and its relationships to Young's modulus. In Section 3, comparisons between the GLNSM and the previous model validate the

relationships which have been derived in Section 2. The final section presents the conclusion of the research.

2. Simulation Method

I. Immersed boundary lattice Boltzmann method

Immersed-boundary lattice Boltzmann method is a numerical method which combines the lattice Boltzmann method (LBM) and the immersed-boundary method.

In LBM, a group of lattice nodes are used to represent fluid. Each node has distribution functions f_σ and discrete velocity $\boldsymbol{e_\sigma}$, where σ depends on the chosen lattice model. The Boltzmann equation with Bhatanaga-Gross-Krook single relaxation time is

$$f_\sigma(\boldsymbol{r}+\boldsymbol{e_\sigma}, t+1) = f_\sigma(\boldsymbol{r}, t) - \frac{1}{\tau}\left[f_\sigma(\boldsymbol{r}, t) - f_\sigma^{eq}(\boldsymbol{r}, t)\right] \tag{1}$$

where τ is the relaxation time and $f_\sigma^{eq}(\boldsymbol{r}, t)$ is the equilibrium distribution function at the position $\boldsymbol{r}$ and the time t as

$$f_\sigma^{eq}(\boldsymbol{r}, t) = \omega_\sigma \rho_f \left[1 + 3(\boldsymbol{e_\sigma}\cdot\boldsymbol{u}) + \frac{9}{2}(\boldsymbol{e_\sigma}\cdot\boldsymbol{u})^2 - \frac{3}{2}(\boldsymbol{u}\cdot\boldsymbol{u})\right] \tag{2}$$

where $\boldsymbol{u}$ is the fluid velocity. In this simulation, the D3Q15 lattice model is applied and the discrete velocity is given by

$$\boldsymbol{e_\sigma} = \begin{cases} (0,0,0), & \sigma = 0 \\ (\pm1,0,0), (0,\pm1,0), (0,0,\pm1), & \sigma = 1 \\ (\pm1,\pm1,\pm1), & \sigma = 2 \end{cases} \tag{3}$$

and the weight coefficient is

$$\omega_{\boldsymbol{\sigma}} = \begin{cases} \frac{2}{9}, & \sigma = 0 \\ \frac{1}{9}, & \sigma = 1 \\ \frac{1}{72}, & \sigma = 2 \end{cases} \tag{4}$$

The fluid density ρ_f and the momentum density $\rho_f \boldsymbol{u}$ are given by

$$\rho_f = \sum_\sigma f_\sigma \tag{5}$$

$$\rho_f \boldsymbol{u} = \sum_\sigma f_\sigma \, \boldsymbol{e_\sigma} \tag{6}$$

The kinematic viscosity ν is related to the relaxation time τ and given by

$$\nu = \frac{1}{3}(\tau - \frac{1}{2}) \tag{7}$$

The immersed-boundary method coupled with the LBM was presented by Feng and Michaelides (2004). The fluid nodes are applied to a regular Eulerian grid, so every boundary solid node will not coincide with the exactly adjacent fluid node. Therefore, the fluid velocity at the boundary solid node can be extrapolated from the fluid velocity of the surrounding fluid

nodes by using a discrete Dirac Delta function (Peskin, 2002).

$$D(\boldsymbol{r}) = \begin{cases} \frac{1}{64h^3}(1+cos\frac{\pi\Delta x}{2h})(1+cos\frac{\pi\Delta y}{2h})(1+cos\frac{\pi\Delta z}{2h}), & |\boldsymbol{r}| < 2h \\ 0, & otherwise \end{cases} \quad (8)$$

where the h is the lattice length and $\boldsymbol{r} = (\Delta\boldsymbol{x}, \Delta\boldsymbol{y}, \Delta\boldsymbol{z})$ is a displacement between a boundary solid node and a boundary fluid node. The fluid nodes are within a spherical volume Π of radius of $2h$, centered at a given solid node.

The fluid velocity $\boldsymbol{u_f}$ at the position of the solid boundary node is given by

$$\boldsymbol{u_f}(\boldsymbol{r^b}, t) = \int_{\Pi} \boldsymbol{u}(\boldsymbol{r^l}, t)\, D(\boldsymbol{r^l} - \boldsymbol{r^b}) d\boldsymbol{r^l} \quad (9)$$

where $\boldsymbol{r^b}$ is the boundary solid position and $\boldsymbol{r^l}$ is the position of lattice fluid nodes within the sphere as shown in Figure 1.

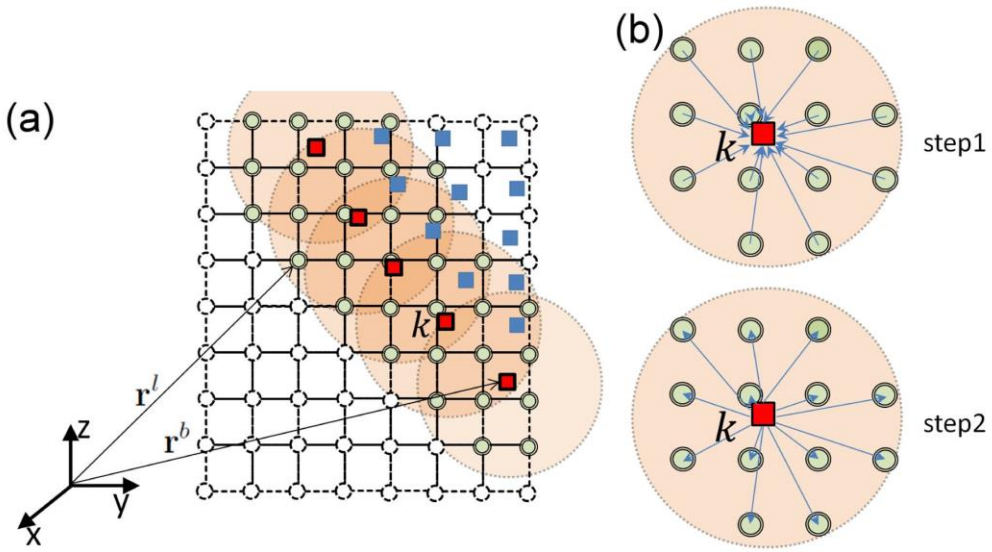

Figure 1: (a) The small circles represent the fluid particles; the squares denote the solid particles; the large circles represent spheres around their central solid particle. (b) Step 1 shows that the flow velocities of fluid particles are interpolated to their central kth solid particle and step 2 shows that the reaction force of the kth boundary solid particle on the fluid is interpolated to its surrounding fluid particles. The arrows denote the interpolation from the fluid to the solid particle positions in step 1 and from the solid to the fluid particle positions in step 2. The figure is from Wu et al. (2014).

Only a part of particles on a plane are shown in Figure 1 to illustrate the interaction between fluid and solid particles in a three dimensional space. The small circles represent the fluid particles and the squares denote the solid particles. The squares with the thicker edges are the boundary solid particles which directly interact with their surrounding fluid particles within a sphere. For example, the velocities $\boldsymbol{u}(\boldsymbol{r^l}, t)$ of the fluid particles around the kth solid boundary particles (see Figure 1(a)) are interpolated to the kth particle position in step 1 (see

Figure 1(b)) to have $\boldsymbol{u_f}(\boldsymbol{r^b}, t)$ using Eq. (9). Under the non-slip condition, the boundary solid node velocity is equal to the fluid node velocity, and thus the momentum difference represents the interaction force $\boldsymbol{F}^{int}$ on the solid boundary over one time step as follows

$$\boldsymbol{F}^{int}(\boldsymbol{r^b}, t) = \rho_f(\boldsymbol{u_f}(\boldsymbol{r^b}, t) - \boldsymbol{u_s}(\boldsymbol{r^b}, t-1)) \tag{10}$$

Next, the discrete Dirac delta function is used again to distribute the reaction force on the surrounding fluid nodes by

$$g(\boldsymbol{r^l}, t) = -\int_{\Gamma} \boldsymbol{F}^{int}(\boldsymbol{r^b}, t) D(\boldsymbol{r^l} - \boldsymbol{r^b}) d\boldsymbol{r^b} \tag{11}$$

where g is the distributed reaction force and Γ is a spherical volume of a radius of $2h$, located at $\boldsymbol{r^l}$. The force distribution process is illustrated in step 2 of Figure 1(b). Finally the reaction force term is added to the Boltzmann equation as follows

$$\begin{aligned} f_\sigma(\boldsymbol{r} + \boldsymbol{e_\sigma}, t+1) = f_\sigma(\boldsymbol{r}, t) - \frac{1}{\tau}\left[f_\sigma(\boldsymbol{r}, t) - f_\sigma^{eq}(\boldsymbol{r}, t)\right] \\ +3\omega_\sigma(g \cdot \boldsymbol{e_\sigma}) \end{aligned} \tag{12}$$

II. Generalized lattice spring model

In mesoscopic scale, the inter-particle force can be regarded as following Hook's law. Based on this idea, Buxton et al. (2005) provided the lattice spring model (LSM) to represent elastic structures. In addition, Wu et al. (2014) have presented the generalized lattice spring model (GLSM), which used angular bonds instead of diagonal spring to treat bending deformation. The model consists of three parts as follows. First of all, a solid body is discretized into particles and the solid particles space regularly. Secondly, two adjacent particles are linked by a harmonic spring. In this way, the harmonic spring energy U^s acted on the ith node is give by

$$U^s = \frac{1}{2} k_s \sum_j (\boldsymbol{r}_{ij} - \boldsymbol{r}_{0ij})^2 \tag{13}$$

where k_s is the spring coefficient; $\boldsymbol{r}_{0ij}$ is the equilibrium length of the spring between two neighboring particles i and j; j is nearest neighboring solid particle of the ith solid particle; $\boldsymbol{r}_{ij} = \boldsymbol{r}_i - \boldsymbol{r}_j$. Three adjacent particles have a set of angular bond. The angular energy U^a is given by

$$U^a = \frac{1}{2} k_{\mathrm{a}} \sum_j \sum_{\mathrm{k,k\neq j}} (\theta_{ijk} - \theta_{0ijk})^2 \tag{14}$$

where k_{a} is the angular coefficient; j, k are the nearest neighboring solid particles of ith solid particle; θ_{ijk} is the angle between the bonding vectors $\boldsymbol{r_{ij}}$ and $\boldsymbol{r_{ik}}$; θ_{0ijk} is the corresponding equilibrium angle.

The spring force is a two-body central force which allows either extension or compression between two solid particles, and the angular force is a three-body force which can handle bending deformation accurately. The sketch of GLSM is shown in Figure 2.

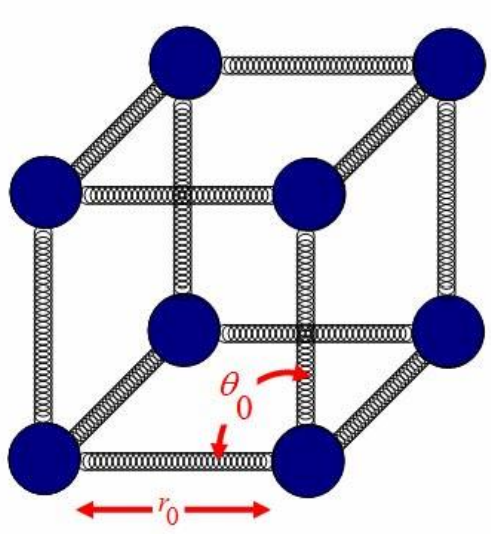

Figure 2: The solid particles are located in a cubic lattice and the particle lattices are linked by springs and angular bonds. The figure is from Wu et al. (2014).

The elastic force $\boldsymbol{F}_i$ on the ith solid particle can be computed from the gradient of the total energy.

$$\boldsymbol{F}_i = -\nabla(U_i^s + U_i^a) \tag{15}$$

The total force $\boldsymbol{F}_T^i = \boldsymbol{F}_i + \boldsymbol{F}^{int}$ drives the solid particle to move. The leap frog algorithm has been used to update the position and velocity of each solid particle at each time step by using Newtonian mechanism. The details about the leap frog algorithm are referred to in Chapter 3 of the book by Allen and Tildesley (1987).

III. Generalized lattice nonlinear spring model

The generalized lattice nonlinear spring model (GLNSM) is similar to the generalized lattice spring model (GLSM). The only difference is that the harmonic spring is replaced by a non-linear spring force, which is a combination of FENE and Lennard-Jones potential. For the ith particle, the non-linear potential is given by

$$U_i^{ns} = U_i^{FENE} + U_i^{LJ} \tag{16}$$

where U_i^{FENE} is the FENE potential and U_i^{LJ} is the Lennard-Jones potential. They are

$$U_i^{FENE} = \begin{cases} \sum_j -\frac{1}{2} K R_0 ln[1 - (\frac{\boldsymbol{r}_{ij}}{R_0})^2], & \boldsymbol{r}_{ij} < R_0 \\ \infty, & \boldsymbol{r}_{ij} \geq R_0 \end{cases} \tag{17}$$

$$U_i^{LJ} = \begin{cases} \sum_j 4\eta\,[(\frac{\sigma}{\boldsymbol{r}_{ij}})^{12} - (\frac{\sigma}{\boldsymbol{r}_{ij}})^{6}], & \boldsymbol{r}_{ij} < R_c \\ 0, & \boldsymbol{r}_{ij} \geq R_c \end{cases} \tag{18}$$

where R_0 is the maximum of length of bonds, K is the non-linear potential coefficient, σ is the distance at which the Lennard-Jones potential is equal to zero, η is the potential depth of Lennard-Jones potential, and R_c is the cutting radius of U_i^{LJ}. According to Kremer and Grest (1990), the relationships between parameters are usually set up as follows

$$R_0 = 1.5\sigma \tag{19}$$

$$K = \frac{30\eta}{\sigma^2} \tag{20}$$

Because U_i^{LJ} is created by the FENE potential plus Lennard-Jones potential, the equilibrium distance r_{eq} should have the minimum potential as shown in Figure 3.

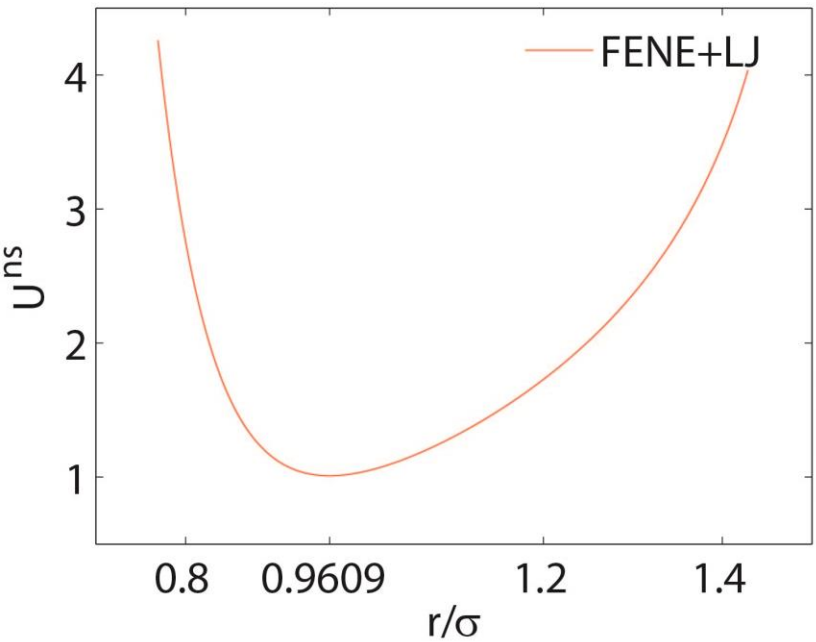

Figure 3: The FENE-LJ potential as a function of the ratio of r to σ. The minimum potential is at $r/\sigma = 0.9609$.

Therefore, the r_{eq} is related to σ as follows and the details are described in Appendix A.

$$r_{eq} = 0.9609\sigma \tag{21}$$

The harmonic spring can be extended without limitation, whereas the FENE-LJ (non-linear) spring is restricted by maximum length of bonds R_0, and usually less 1.2 σ (Kremer & Grest, 1990). The non-linear spring can represent the physical properties more precisely as well. However, the relationship between microscopic parameters and Young's modulus is reported in literature. In order to obtain the relationship, a strain ε and $\boldsymbol{r}_0 = \boldsymbol{r}_{\mathrm{eq}}$ are assumed, and thus the force is expanded as a series of power of strain ε at $\boldsymbol{r} = \boldsymbol{r}_0$. That is

$$\boldsymbol{F}(\boldsymbol{r}_0 + \boldsymbol{r}_0\varepsilon) = -\nabla U^{NS}(\boldsymbol{r}_0 + \boldsymbol{r}_0\varepsilon) \cong -\frac{942.8515\eta}{\sigma}\varepsilon + O(\varepsilon^2) \tag{22}$$

where $\boldsymbol{r}_0\varepsilon$ is a small deformation. The first result term

$$-\frac{942.8515\eta}{\sigma}\varepsilon \tag{23}$$

is proportional to the strain ε and higher order terms are neglected. In Young's modulus

$$E = \frac{F/A}{\varepsilon} \tag{24}$$

F is the external force and A is the area. In this model, the area A is equal to ${r_0}^2$ as shown in Figure 4, so the Young's modulus is as follows

$$E \cong \frac{1021.1439\eta}{\sigma^3} \tag{25}$$

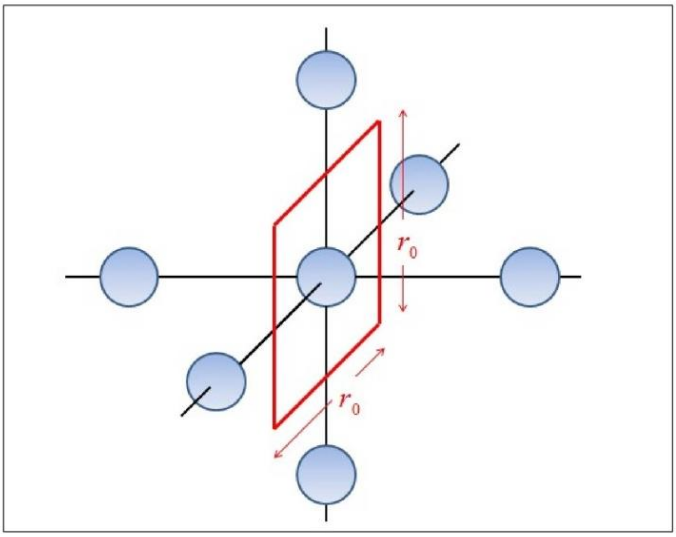

Figure 4: The unit area of each node is a square (the red square) and its value is ${r_0}^2$. The figure is from Wu et al. (2014).

3. Results

In order to validate the results in the previous section, the locomotion of a filament in fluid is introduced. In Wu et al. (2014), the GLSM has been proved that its results are reliable, so we can use the equilateral parameters and compare the results between the GNLSM and GLSM.

An elastic cylindrical filament with the length $L = 50$, the radius $r = 2.5$ is constructed, and the simulation box $(N_x, N_y, N_z) = (64,416,400)$. The structure coefficients $(k_s, k_a) = (0.26,0.025)$ which represent Young's modulus $E = 0.26$. The equilateral stiffness

parameters in GNLSM are $\eta = 0.000287$ and $\sigma = 1.0407$, which has the same Young's modulus. Both the density of solid ρ_s and the density of fluid ρ_{f} are set to 1, $\rho_s = \rho_f = 1$. All above parameters are presented by non-dimension.

A driven point is located at the center of the cross section of the right end of the filament. The motion of the driven point follows a harmonic function

$$z = z_0 sin\omega t \tag{26}$$

where amplitude $z_0 = 0.1L$, $\omega = 2\pi f$ and driven frequency $f = 8Hz$. The maximum velocity for driven point is $v_{max} = z_0\omega$, and the definition of Reynolds number is

$$Re = \frac{v_{max\,L}}{\nu} \tag{27}$$

where ν is the viscosity of fluid. All cases are at $Re = 10.21$.

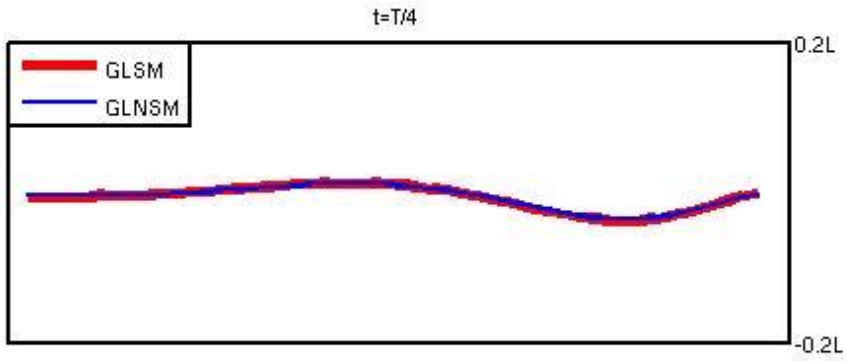

Figure 5: The comparison between the GLSM (red line) and GLNSM (blue line) at step is equal to $\mathrm{T}/4$.

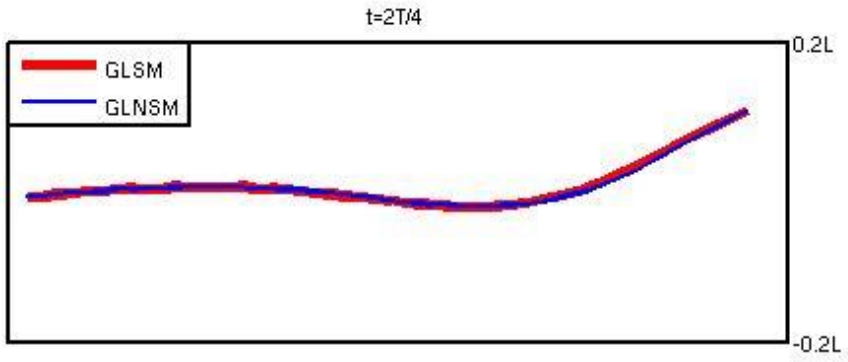

Figure 6: The comparison between the GLSM (red line) and GLNSM (blue line) at step is equal to 2T/4.

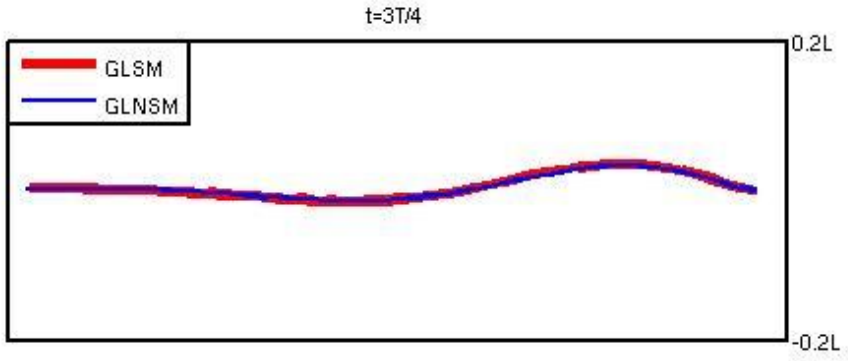

Figure 7: The comparison between the GLSM (red line) and GLNSM (blue line) at step is equal to 3T/4.

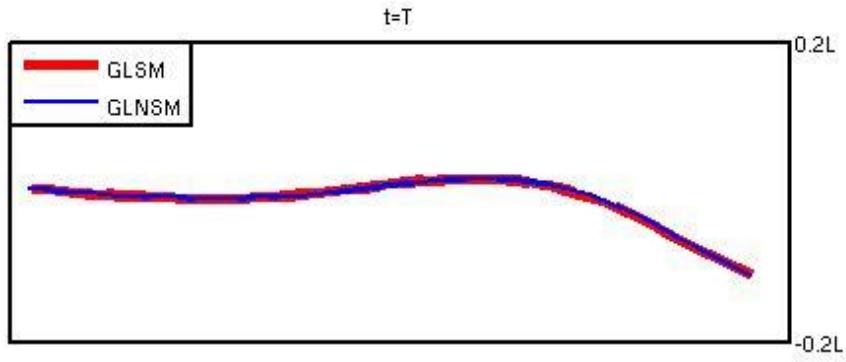

Figure 8: The comparison between the GLSM (red line) and GLNSM (blue line) at step is equal to T.

In Figure 5, Figure 6, Figure 7 and Figure 8, the wave patterns of the GLNSM agree well with the patterns of the GLSM. The results show that Eq. (25) can represent Young's modulus precisely by the GLNSM.

4. Conclusion

In the present work, the generalized lattice nonlinear spring model (GLNSM) has been introduced into lattice Boltzmann simulation. The Young's modulus, which is a significant property of matters to describe extension, has been derived from FENE-LJ potential for a cubic lattice solid structure for the first time. A comparison between the GLNSM and generalized lattice spring model (GLSM) is made. The simulation results validate the GLNSM and its relationship to Young's modulus.

Appendix A

In order to investigate the relationship between Young's modulus and GLNSM, the force function is necessary which can be derived from the derivative of potential.

$$F^{NS} = -\nabla U^{NS}$$

The parameters are set as Eqs. (19) and (20). The results of the potential U^{NS} and the force F^{NS} are shown as follows

$$U^{NS} = \frac{1}{2}\left(30\frac{\eta}{\sigma^2}\right)(1.5\sigma)^2\, ln\left[1-\left(\frac{r}{1.5\sigma}\right)^2\right] + 4\eta[\left(\frac{\sigma}{r}\right)^{12} - (\frac{\sigma}{r})^6]$$

$$F^{NS} = -\frac{30\eta r}{\sigma^2(1-\frac{4}{9}\frac{r^2}{\sigma^2})} - 4\eta(-\frac{12\sigma^{12}}{r^{13}} + \frac{6\sigma^6}{r^7})$$

In addition, the equilibrium distance r_{eq} is the distance at which the potential U^{NS} is the minimum or the force F^{NS} is equal to zero. Therefore, we solve the equation $\mathrm{F^{NS}} = 0$ numerically and the result is shown in Eq. (21) and Figure 3.

References

Allen, M. P., & Tildesley, D. J. (1987). Computer simulation of liquids. New York: Oxford University Press.

Buxton, G. A., Verberg, R., Jasnow, D., & Balazs, A. C. (2005). Newtonian fluid meets an elastic solid: coupling lattice Boltzmann and lattice-spring models. *Physical Review E*, *71*(5), 056707.

Feng, Z. G., & Michaelides, E. E. (2004). The immersed boundary-lattice Boltzmann method for solving fluid–particles interaction problems. *Journal of Computational Physics*, *195*(2), 602-628.

Kremer, K., & Grest, G. S. (1990). Dynamics of entangled linear polymer melts: A molecular-dynamics simulation. *The Journal of Chemical Physics*, *92*(8), 5057-5086.

Peskin, C. S. (2002). The immersed boundary method. *Acta numerica*, *11*, 479-517.

Tirion, M. M. (1996). Large amplitude elastic motions in proteins from a single-parameter, atomic analysis. *Physical review letters*, *77*(9), 1905.

Urgessa, Z. N. (2007). Molecular Dynamics Simulation of Polymer Chain.

Wu, T. H., Guo, R. S., He, G. W., Liu, Y. M., & Qi, D. (2014). Simulation of swimming of a flexible filament using the generalized lattice-spring lattice-Boltzmann method. *Journal of theoretical biology*, *349*, 1-11.